



# Reducing Noise Generated from a Wind Turbine Blade by Pitch Angle Control using CFD and Acoustic Analogy

M. Maizi<sup>1,2†</sup>, R. Dizene<sup>2</sup> and M. C. Mihoubi<sup>3</sup>

<sup>1</sup> Centre de Développement des Energies Renouvelables, CDER, 16340, Algiers, Algeria

<sup>2</sup> Université des Sciences et de Technologie Haouari Boumdienne (USTHB), Alger, Algérie

<sup>3</sup> Fraunhofer Institute for Wind Energy and Energy System Technology (IWES), 26129 Oldenburg, Germany,

†Corresponding Author Email: [mohamedmaizi@yahoo.fr](mailto:mohamedmaizi@yahoo.fr)

(Received November 23, 2016; accepted March 21, 2017)

## ABSTRACT

Investigation of the effects blade pitch angle on noise emission from a horizontal axis wind turbine is the goal of this paper. To understand the flow around blade wind turbine, and to reduce noise emission in order to respect noise regulation, especially a residential area, three different pitch angles  $0^\circ$ ,  $3^\circ$ , and  $6^\circ$  are tested, using computational aerodynamic and aero acoustic methods. Three dimensional flow simulations are carried out with two unsteady CFD simulations URANS, DES used to calculate the near-field flow around a HAWT of NREL Phase VI small scale. The far field noise is predicted from the simulated sources by the Ffowcs William and Hawkins analogy, and compared and validated with available test data for a small-scaled model of the NREL Phase VI. The comparison demonstrates a generally good agreement between DES predicted and measured noise levels. It can be seen that the noise emission increases by decreasing pitch angle. Moreover, the pitch angle control has a significant effect on the noise emission especially in the intermediate frequency range. We show that it is possible to reduce the noise level by control pitch angle without losing too much the power.

**Keywords:** Wind turbine aerodynamics; DES; URANS simulation; Computational fluid dynamics; Noise; Pitch angle and control noise.

## NOMENCLATURE

D	blade diameter	$P_{ref}$	acoustic reference pressure
ID	Inner Domain.	r	local radius for the span wise section $u_i$
KARI	low speed wind tunnel, aerospace recherché	R	radius of blade
$L_w$	sound power level	SPL	Sound Pressure Level
N	rotational speed	$S_{ref}$	acoustic reference power
$N_g$	Grid number	$S_{ref}$	sound reference power
OD	Outer Domain	$S_w$	sound power at the source
p	local pressure	$U_\infty$	wind speed
$P'$	acoustic pressure	$\rho$	density of air
$p_{re}$	reference pressure	$\Omega$	rotational angular velocity

## 1. INTRODUCTION

In recent times, Due to the increasing consumption of energy, there has been a rapid development of wind energy all over the world. The worldwide total capacity of wind energy installed approximately 392 GW by the end of June 2015 (WWEA (2015)). The principal objective in the past is based on the

productivity global of wind turbine. However, wind energy also has several minuses, which are hindering its global use (AbdelSalam (2014)). One of its major problems is noise because it directly affects nearby residents, especially aerodynamic noise, emitted from the wind turbine blades. Noise is frequently cited as a major obstruction for the general acceptance of wind energy. For a modern large wind

turbine (WT), there is an urgent need to predict aerodynamic noise generated by wind turbines and to find noise reducing design concepts in order to increase public acceptance of wind energy (Arakawa and Oliver 2005). Aerodynamic noise from the blades is the dominating noise source, provided that mechanical noise is adequately eliminated (Wagne and Bareiss 1996).

The sources of aerodynamic noise can be broadly classified as discrete frequency (tonal) noise and broadband noise (Burton and Sharpeand 2001). The tonal noise is generally low frequency, due to the disturbance in the flow caused by the blade rotating (thickness noise), and associated force fluctuations (loading noise). However, the broadband noise is higher frequency originates from the interaction between natural atmospheric turbulence and wind turbine blades, for the generation of this noise, the interaction of turbulence with both the leading and trailing edges is important (Gwang and al 2007).

Tadamasa (2011) had been realized in modeling wind turbine noise using Unsteady Reynolds Averaged Navier Stokes (URANS) methods, particularly the low frequencies.

However, URANS techniques have an insufficient capacity for predicting the noise emission especially at high frequencies. In order to capture all small turbulence structures specially in the acoustic problem, the DNS (direct simulation) method is more preferably, which resolves all small turbulence structures without any form modelling. However, DNS is very costly in terms of computation time, it needs a very refined mesh resolution to resolve all turbulent length scales. Spalart (2000) gave an approximation about the grid number for resolving the flow around aircraft using DNS at Reynolds number 107 is around of 1016 nodes. Using this method in wind turbine cases is impossible due to massive computational cost. The next possibility is to use a LES model, which has a lower cost than a DNS method and is able to model small turbulent structures to a certain level.

Arakawa and al (2005) carried out noise numerical simulation prediction of wind turbine blade noise, using LES model in order to reduce tip blade noise. Due to the fine grid employed in LES modelling, the acoustic near field of the entire blade has the total number up to 300 million nodes are performed on the Earth Simulator with 112 processors in parallel. The simulation was carried out only for a total time of 50 milliseconds with the blade rotation of 20.4 degrees. However, it is seen that their results differ significantly from experimental noise measurements due to the short time period used to obtain a reliable sound spectrum.

LES near-wall mesh requirements render it impractical for industrial flows. Detached Eddy Simulation (DES) offers a more practical solution, and is often no more expensive than URANS (Burton 2001). On other hand, Mo and Lee (2011) used hybrid method analogy acoustic with LES to predict the aero-acoustic noise from the NREL phase VI wind turbine (2 blade with tower). Their results indicated that there is a significantly close relation

between the quadrupole noise by different structures size and the increase of wind speeds. The aerodynamic noise was modeled below frequency 500 Hz; however, the sensibility hearing range of the human ear is 20 Hz-20 kHz.

Cho and al (1997) carried out wind tunnel test noise measurements for the 12% scaled model of NREL Phase VI wind turbine, they used an acoustic array of 144 microphones. They applied Time based beamforming method to identify the noise source position on the blade wind turbine. Their results show that the dominant noise source moves to the blade tip as frequency increases, and in the stall condition, the noise emission from a wind turbine is much higher at low frequency below 2 kHz. Sahan and al (2015) predicted the noise radiated from the rotating horizontal axis wind turbine blades with LES model. They used just annular computational domain around tip blade in order to reduce the simulation cost. There are different methods instigated for reducing noise emission generated from wind turbines. Many studies have focused on wind turbine blade modification to minimize the noise emission with minimum impact on aerodynamic performance (Oerlemans 2008 and Göçmen 2012). The effect of serrated trailing edges of the blades on noise emission (Herr (2006), Gruber and al 2011).

Another method base on the active control were used to reduce the noise emission during turbine operation, by varying the rotation speed of the wind turbine, pitch angle and the generator torque. Control of this parameters used to settle the rotor tip speed and the blade angle of attack in order to reduce the noise emission (Shaltout and al 2013).

Leloudas and al (2007) carried out a parametrical study to optimize the performance and noise emissions from a 2.3 MW Wind Turbine by changing tip speed and pitch setting using the acoustic model is based on the Blade-Element Momentum (BEM) technique and semi empirical code noise. Their results show that there is a possibility to reduce the noise emission level up to 2 dB(A) without sacrificing too much the output power. From the previous summary of the literature, it is found the pitch angle of the wind turbine blades also has a significant influence on noise emission.

The main intention of the paper is an investigation of the effects blade pitch angle on noise emission from wind turbine using coupled aerodynamic and aero-acoustic model in order to reduce noise emission generated from wind turbines. The aerodynamic and near-field noise around the wind turbine generator is directly analyzed using two models RANS and DES model. The far-field noise is calculated at the specific locations away from the wind turbine, using FW-H analogy, and compared and validated with available test data for a small-scaled model of the NREL Phase VI.

## 2. DETACHED EDDY SIMULATION

In a challenge to improve the capacity of turbulence models in heavily separated regions. The Detached

Eddy Simulation (DES) is a hybrid scheme, was proposed by Spalart (1994), which combines a conventional Reynolds averaged Navier-Stokes simulation (RANS) with elements of Large Eddy Simulations (LES) methods. The RANS method is used to covering the boundary layer in the near wall regions. However, switching to the LES mode in separated flow regions. Based on the modest costs of a RANS in the boundary layer region is combined with the advantages of a LES in the detached flow regions. DES relies on the relationship of the turbulent length-scale computed from the model of the turbulence and the local grid spacing. If the grid spacing is sufficiently smaller than the turbulent length-scale, the model switches to the LES mode.

The code ANSYS CFX is also used for the DES simulation. This program uses an SST-DES formulation based on the idea from Strelets which is extended with a zonal limiter to avoid grid induced separation inside the boundary layer. Strelets also noted that a switch between different numerical treatments should be employed to avoid excessive numerical diffusion in the LES mode. In CFX a second order upwind scheme with numerical advection correction is used in the RANS and a central difference scheme in the LES region is used. The time integration is done by a second-order backward Euler scheme.

### 3. ACOUSTIC ANALOGY METHODS

The aero acoustic prediction model is based on the Ffowcs Williams-Hawkings (FW-H) equation (Ffowcs and Hawkings 1996), which is the most general formulation of the Lighthill acoustic analogy (Lighthill 1952), and it treats the problem of sound generated by a body in arbitrary motion in both time and frequency domains. FW-H equation has been widely used for the successful prediction of helicopter rotors, propellers and fans. The FW-H equation is based on an analytical formula, which relates the far-field pressure to integrals over a closed surface that around all the acoustic sources. This equation (FW-H) is a rearrangement of continuity equation and Navier-Stokes (N-S) equations into an inhomogeneous wave equation with sources of sound (monopole, dipole and quadruple) as expressed in the form of Eq. (1)

$$\begin{aligned} \frac{1}{a_0^2} \frac{\partial^2 p'}{\partial t^2} - \nabla^2 p' = & \\ \frac{\partial}{\partial t} [(\rho_0 V_n + \rho(U_n - V_n))\delta(f)] & \quad (1) \\ - \frac{\partial}{\partial x_i} [(P_{ij} n_j + \rho u_i(U_n - V_n))\delta(f)] & \\ + \frac{\partial^2}{\partial x_i \partial x_j} [T_{ij} H(f)] & \end{aligned}$$

The formulation (1) is a well-validated method that is used extensively in rotorcraft aero-acoustics (Schultz 1994, Spalart 1994). The first term on the right side is a monopole source caused by unsteady mass injection, the second term is a dipole source by unsteady external forces, and the third term is a

quadruple source caused by unsteady shear stresses.  $p'$  is the sound pressure at the far field. ( $f=0$ ) denotes a mathematical surface introduced to “surround” the exterior flow problem ( $f > 0$ ) in an unbounded space, which facilitates the usage of generalized theory and the free-space Green equation to obtain the solution.

The surface ( $f = 0$ ) corresponds to the source (emission) surface (blade and shaft),  $n_j$  is the unit normal vector pointing toward the exterior region ( $f > 0$ ).  $a_0$  is the far-field sound speed, and  $T_{ij}$  is the Lighthill stress tensor as defined :

$$T_{ij} = \rho u_i u_j + P_{ij} - a_0^2 (\rho - \rho_0) \delta_{ij} \quad (2)$$

$u_i$  is fluid velocity component in the  $i$  direction, unit fluid velocity component normal to the surface  $f=0$ ,  $V_{ij}$  is the surface velocity component in the  $x_i$  direction,  $V_n$  is surface velocity component normal to the surface.

$\delta(f)$  is the Dirac delta function,  $H(f)$  is Heaviside function,  $P_{ij}$  is the compressive stress tensor. (Jang-oh 2011).

### 4. TURBINE GEOMETRY

The available CFD solver, ANSYS CFX, has been used to calculate the aerodynamic flow parameters, required as an input to the FW-H equations. The validation of the flow solver has been performed on model of the NREL wind turbine. The original model of phase VI is at two blade zero cone angle, the geometry of the blade was detailed in (Scheepers1997) with a diameter of 10 m. The turbine (12% scale model, as shown in Fig. (1)). was tested at KARI low speed wind tunnel, Aerospace Recherche institute (Cho and al (2010)). The NREL wind turbine models are usually used for the numerical validation code due to the accessibility of experimental data at various operating conditions.

Figure 1.b is a view of the baseline Blade NREL Phase VI. The original model of phase VI is at two-blade zero cone angle, the geometry of the blade is based on the airfoil S809 from root to tip. The blade is highly twisted at the root region with positive twist angle  $20.04^\circ$  and the tip region has a negative twist angle  $-2.15^\circ$ . The radius of the blades is 5.029 m and the rated power of the wind turbine is 20 kW.

### 5. COMPUTATIONAL DOMAIN AND GRID

In the current work, the tower of wind turbine and the ground effect are neglected. Which is a fair approximation for HAWT rotor simulation.

The computational domain is composed of two cylindrical sub-domains; one outer stationary domain with coarse mesh.

The computational domain for NREL phase VI domain calculation is enclosed between a smaller inner cylinder and an outer semi-cylinder with radius equal to 5 times the rotor diameter. Thus, the field is extended to 10 rotor diameters downwind of the turbine.

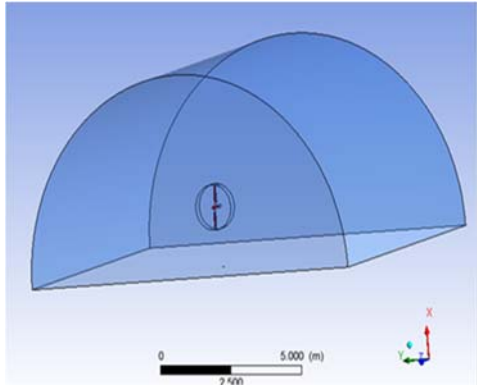


Fig. 1. a Computational domain.

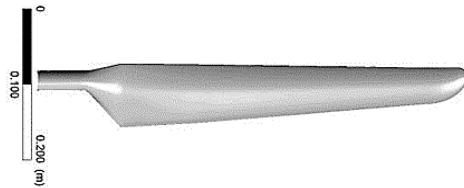


Fig. 1. b Blade shape of the NREL Phase VI Rotor.

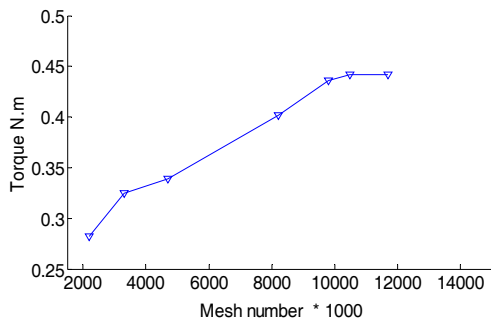
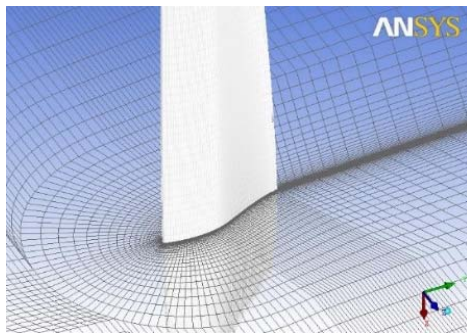
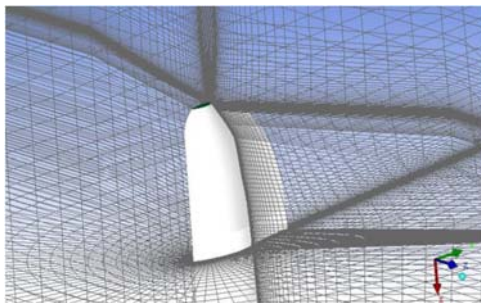


Fig. 2. Mesh sensitivity.



Grid near the blade surface



Tip Blade mesh

Fig. 3. Computational meshes.

Table 1 Grid properties of different cases

ID N*10 <sup>3</sup>	OD N*10 <sup>3</sup>	FIRST node *10 <sup>-5</sup>	EXP ratio	Ng CHORD wise	Ng In BL	Ng Span wise
6400	3400	0.2	1.2	110	35	126

ID: Inner Domain, OD: Outer Domain

The pre-processor Ansys ICEM is used to create the volume mesh. The detail of nodes number of the numerical grid is shown in table.1, consisting of hexahedral grids over the total domain, as shown in Fig. (3). For the investigation of the meshing effect on the numerical results, seven different grid numbers were used; Fig. (2) shows the relationship between the torque and the mesh number.

All the calculations were carried out in workstation HP Z820 with 96 GB Ram and 24 processors. The working fluid for this analysis is the air with a density equal to the reference value in the experimental data, which is 1.2 kg/m<sup>3</sup>. Regarding the boundary conditions, a velocity condition with a turbulent intensity of 1% is applied at the upstream boundary where the flow enters the cylindrical domain, and an ambient pressure condition is applied at the downstream point at which the flow leaves the cylindrical domain. The nominal rotation (NREL phase VI scaled model) speed is 600 rpm and three different pitch angles 0°, 3°, and 6°, are used for the rotor blade calculations. The frozen rotor interface was used between the outer and inner region. The no-slip wall condition is assigned to the rotor blade surface and the pressure outlet condition to the condition to the downstream wind extreme of the field.

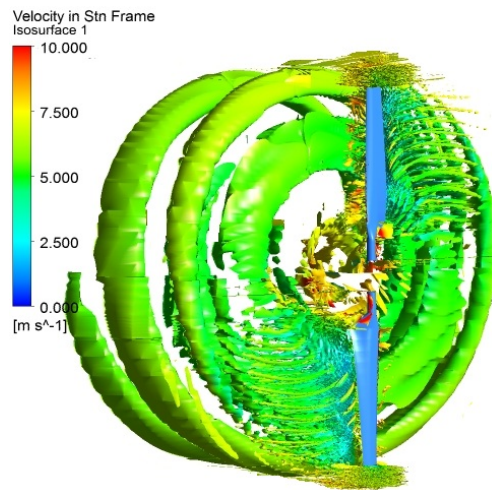


Fig. 4. Instantaneous iso-surface vorticity at 125 s<sup>-1</sup>.

## 5. RESULTS

The CFD code ANSYS CFX is used for all the calculations presented in this work. In order to validate the numerical results, experimental data are used from rapport: unsteady aerodynamics

experiment in the NASA-Ames wind tunnel (Simms 2001). The numerical pressure coefficient distribution is presented and compared with experimental results from NREL phase VI full model under velocity condition  $7 \text{ m.s}^{-1}$ , rotating velocity 72 rpm (30%, 47 %, 63 %, and 80%) span wise locations, respectively. The calculated pressure coefficient is defined by Eq. (3):

$$C_p = \frac{P - P_\infty}{\frac{1}{2} \rho (U_\infty^2 + (\omega r)^2)} \quad (3)$$

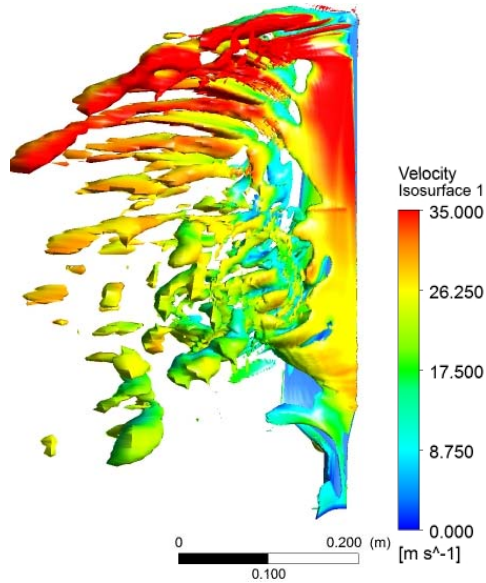


**Fig. 5. Vorticity at  $7.4 \text{ m s}^{-1}$  from the DES model.**

Where,  $U_\infty$  is wind speed;  $P$ : local pressure;  $P_\infty$  reference pressure;  $\rho$ : density of air;  $\omega$  rotational angular velocity;  $r$  the local radius for the span wise section. For the purpose of verification, numerical computational data at the same points on the blade surface as in the experiments are taken out. Fig. 8 shows the pressure coefficient on the surface blade for a wind speed  $7 \text{ m.s}^{-1}$  for full model (rotating velocity: 72 rpm).

The pressure coefficient at all span wise sections show good agreement with experimental data. Fig. 7 shows a cross section of velocity and pressure corresponding to the pressure plots, it's clear the flow is attached at the blade surface at wind speed  $7 \text{ m.s}^{-1}$  for wind turbine full scale.

Figure 6 shows the streamlines on the suction side and pressure side of the blade. It can be seen that the flow reversal from the trailing edge to this mid chord limiting streamline and it is moving down the blade towards the tip.

Figure 4 shows the instantaneous iso-surface vorticity on wind turbine blade. It can be observed that the near flow field is characterized by a helical structure of tip vortices; they are shed from the blade tip. Another strong feature of the near wake (see fig 5), it can be identified tip vortex is associated by complex vortical flow structures due to the separated

shear layer and root vortices. It is clearly seen that the DES model is capable of smoothing out mostly all the vortices size. These all vortices are considerate as an important source noise generation.

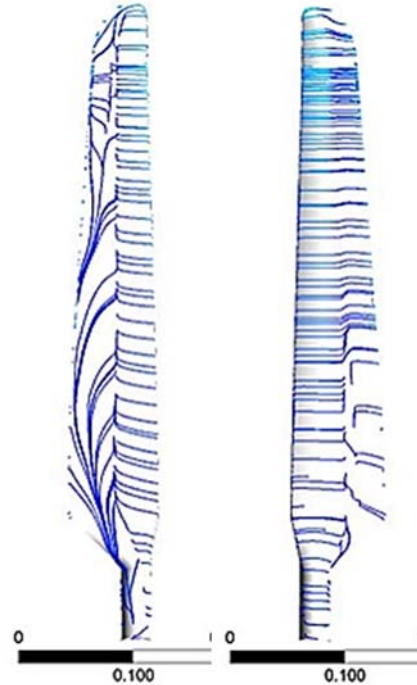


**Fig. 6. Streamline on section side and pressure side at velocity  $5.4 \text{ m.s}^{-1}$  (12% scaled model).**

## 7. AERO ACOUSTIC ANALYSIS

In this section, the aero-acoustic analysis is discussed to evaluate the noise radiated from a scale model with different pitch angle. The flow around the wind turbine blades are calculated using the unsteady flow field on the blade surface extracting from two turbulences models.

The SST-DES model is applied in the present work to investigate the case at rotating velocity speed 600 rpm (12% scale model) with different pitch angle at wind speed  $5.4 \text{ m.s}^{-1}$ . The time step was restricted at  $10^{-5}$  seconds and the simulation was performed for a period time of 0.6 second with approximately 6 rotation blade in order to obtain an accurate prediction. The time of this period is very acceptable to obtain a reliable sound spectrum.

The acoustic power pressure (from a small scale model which was chosen according to available experimental data) of the hybrid RANS-LES and URANS calculations are plotted in Fig. 9 according to the following expression:

$$L_w = 10 \log \left( \frac{S_w}{S_{ref}} \right) \text{ dB} \quad (4)$$

The power level results from the hybrid model are very close to the experimental data mostly for the

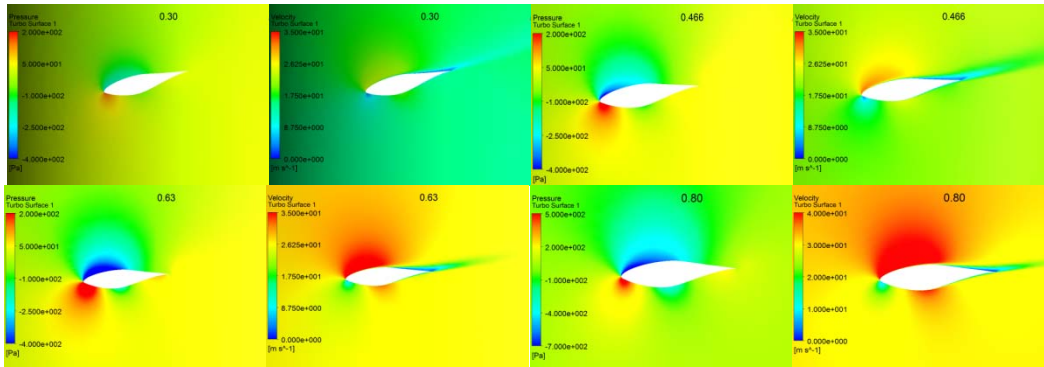


Fig. 7. Pressure section cross (left) and velocity section cross (right) at wind speed  $7 \text{ m.s}^{-1}$ .

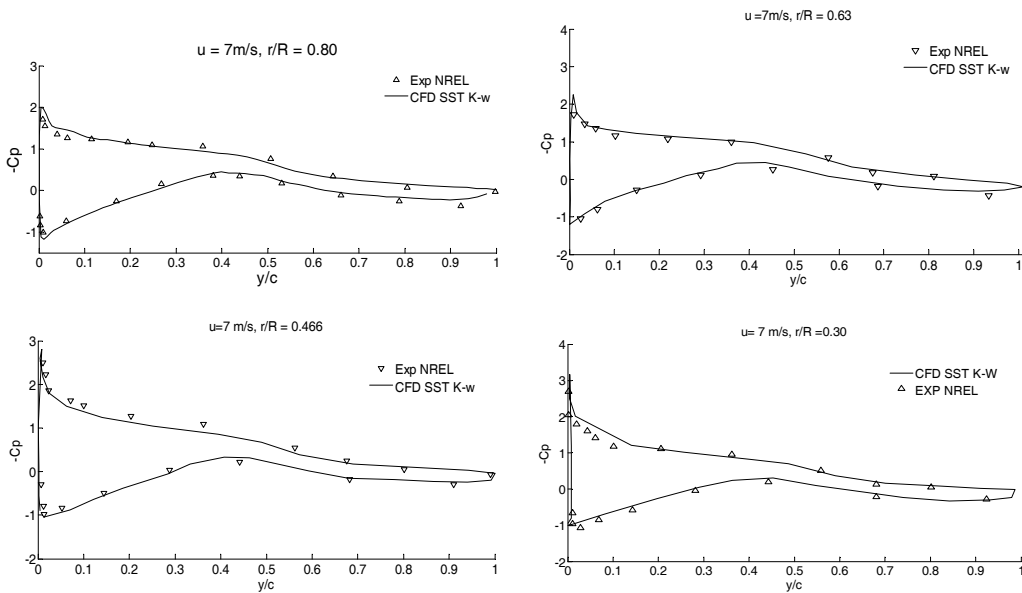


Fig. 8. Comparison between experimental and numerical pressure distribution at different spanwise location.

whole range of frequencies below 1000 Hz. The difference in power pressure level between numerical predictions from the hybrid and experimental measurements was within  $\pm 5 \text{ dB}$  for medium-to high-range frequencies below 1500 Hz. The noise radiation is almost superimposed for the frequencies below 3000 Hz at experimental values.

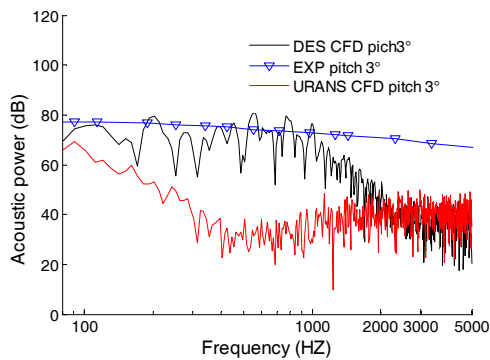


Fig. 9. Sound power pressure level for small scale phase VI pitch  $3^\circ$ .

But there is a big difference in acoustic power between numerical prediction from URANS and experimental measurements arrived at 30 dB for most frequencies.

The simulation using an URANS model (SST) has an apparent weakness to smooth out small turbulence structures. We can suggest the use of a DES model, which provides reasonable good results at medium and high frequency components on the noise spectra.

The noise radiation in this case, where the wind turbine rotor is rotating around 600 rpm.

The observer is located at a reference position  $\theta_r$  according to IEC 61400-11.

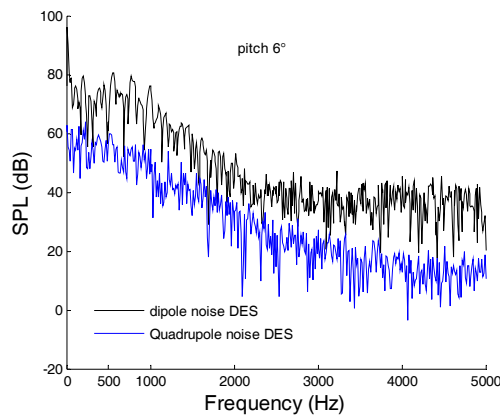
$$\theta_r = H + D / 2 \quad (5)$$

Figure 10 represents sound pressure levels (SPLs) by an FFT analysis. SPLs are expressed by :

$$SPL_s = 20 \log \left( \frac{p'}{p_{ref}} \right) \text{ dB} \quad (6)$$

For the DES model, there is a big significant

difference in the pressure level sound between dipole and quadrupole source for the whole range of frequencies. It is note that the most energy sound emission is of dipole nature.



**Fig. 10. Sound pressures level for small scale phase VI.**

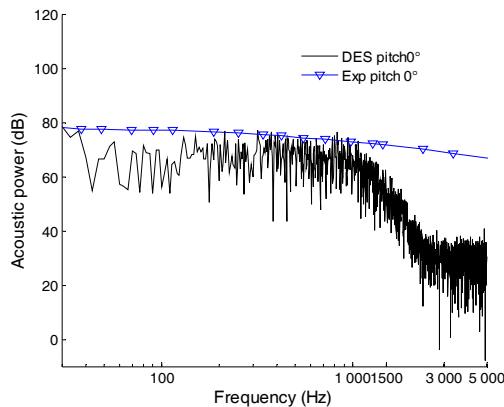


**Fig. 1. 1 Sound power pressure level for small scale phase VI pitch 0°.**

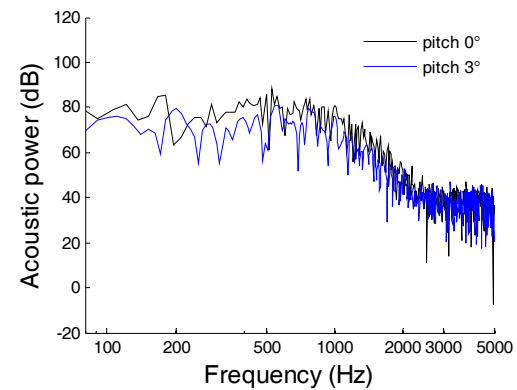
In order to study the effect pitch angle on the wind turbine noise, the noise spectrums from different pitch angles are shown in Fig. 13 and Fig .14 with fixed wind speed  $5.4 \text{ m.s}^{-1}$  and rotating speed 600 rpm.

Figure 12 demonstrates the comparison between acoustic power emission generated from two setting of pitch angle ( pitch $3^\circ$  and pitch  $0^\circ$  ).In the range below 500 Hz, there is a significant reduction on acoustic power (up to 10 dB at 500 Hz) by increasing the pitch angle. After 500 Hz, the noise is slightly reduced by increasing the pitch angle.

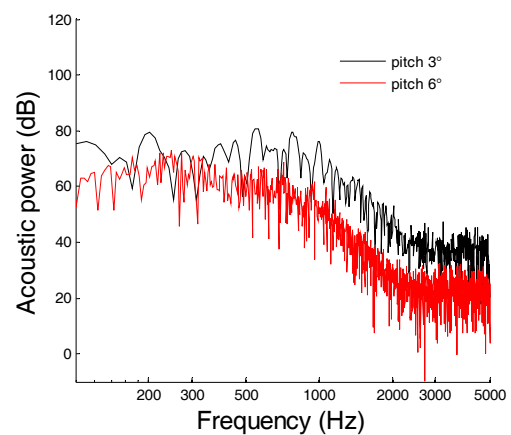
The Fig. 13 shows noise emission at pitch  $6^\circ$  setting is less than noise generated by pitch  $3^\circ$ , we can observe in the range between 250 Hz and 400 Hz, the reduction is not important but above 500 Hz the reduction on acoustic power it is very important (up 15dB in all frequency above 500 Hz).

Figure 14 shows sound pressure level from blade wind turbine at different pitch angle setting, the results indicate that the noise emission increases by decreasing pitch angle. The differences between two settings are mainly observed in the intermediate

frequency range from 300 Hz to 2000 Hz.



**Fig. 12. Sound power level spectra for different blade pitch angle.**



**Fig. 13. Sound power level for pitch angle (3°, 6°).**

A changing in pitch angle causes a changing in the angle of attack. As increasing the angle of attack, the size of the turbulent boundary layer on the suction side of the blade increases, and small structures begin to produce due to the mildly separated flow, and continue to interact with the trailing edge of the blade, the reason of that intense noise generation from wind turbine blade. The results indicated that the SPL shows a strong dependency on the pitch angle.

As the wind speed increases, the boundary layer develops on blade surface, large-scale unsteady structures begin to produce, stall condition occurred, causing a significant level of unsteady flow around the blade see Fig. 5.

These all vortices are considerate as important source noise generation and induce a fluctuation pressure into far-field.

Figures 16 illustrate the pressure fluctuations taken at reference position for a period time of 0.1s, it can be seen that the amplitude of the pressure fluctuations has decreased by increasing the pitch angle setting.

It is shown that a possibility to reduce the sound pressure level by using control pitch angle. It is

important to find the suitable pitch angle for optimal noise control. The major drawback of pitch control noise is effected directly on the power output see table 2. Further table 2, shows that the power production is reduced by 5-7 % with the changing pitch setting.

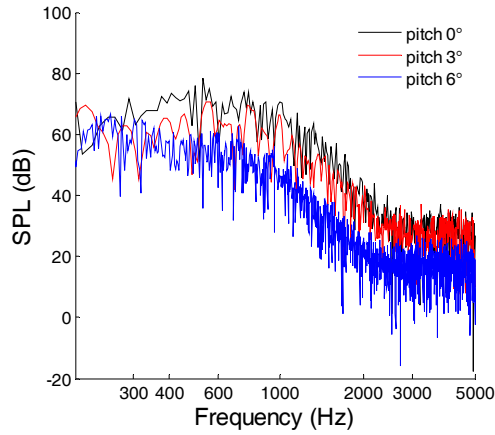


Fig. 14. Sound pressure level for pitch angle (6°, 3°, 0°).

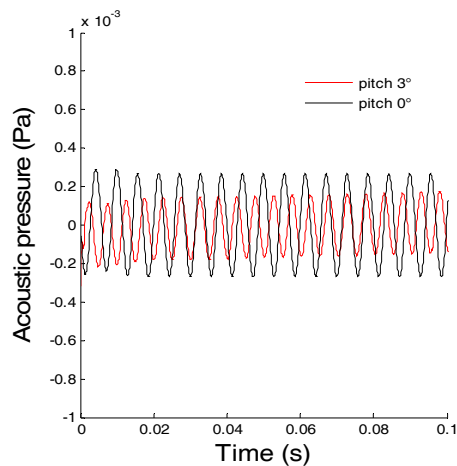


Fig. 15. Acoustic pressure at inlet velocity 5.4 m.s<sup>-1</sup>.

Table 2 Power variation from different pitch angle cases

	Velocity 5.4 m.s <sup>-1</sup>	Velocity 10 m.s <sup>-1</sup>
$P_{3^\circ} - P_{0^\circ} / P_{0^\circ}$	- 0.05	- 0.25
$P_{6^\circ} - P_{0^\circ} / P_{0^\circ}$	- 0.07	-0.125

However, in the most countries, the noise regulation is limited during the night, so it is preferable to take these measures only at night, in order to reduce negative impact on power production.

Figure 16 shows the overall sound pressure level as a function of distance from two-pitch angle, it is clear that the adjustment of the pitch angle has an effect on OASPL of wind turbine.

Depending on this study, it is obvious that the DES model proves perfectly that the dipole noise is the dominant noise source in the whole range of

frequencies especially for the high frequencies in the case of wind turbine noise. The DES model is capable of smoothing out mostly all the structures size better and more accurate than URANS model with lower cost than LES model.

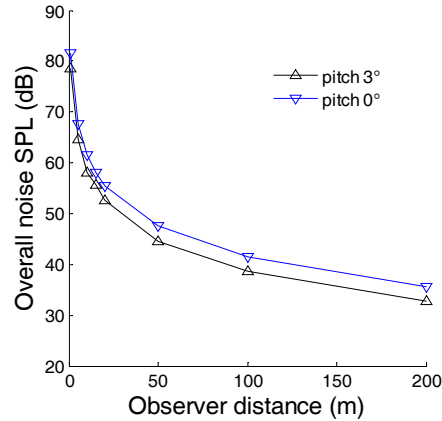


Fig. 16. The overall noise at different observer distance at velocity 10 m.s<sup>-1</sup>.

## CONCLUSIONS

In this work, URANS and DES are tested to predict aerodynamic noise generated from the HAWT of NREL Phase VI small scale. Moreover, the pitch angle control was performed in order to reduce noise emission a residential area with a minimal effect on the output power.

The far-field acoustics was computed from an integral form solution to the Lighthill equation, developed by Ffowcs-Williams and Hawkings. The noise evaluation is obtained by using the pressure fluctuations on the wind turbine blades computed from two turbulence models (URANS and DES) based computational fluid dynamics (CFD) solver. The aerodynamic simulation results were validated against experimental measurements of the NREL phase VI wind turbine full model. The results show that although this model cannot be used for exact prediction of noise levels radiated from wind turbine, the use of a DES model, which provides reasonable good results at high frequency components on the noise spectra. The DES model is capable of smoothing out mostly all the structures size better and more accurate than an URANS model with lower cost than LES model. The results convincingly show the acoustical field close to the wind turbine is dominated by dipole source noise.

Moreover, the results indicate that the noise emission from wind turbine blade have a strong dependence on pitch angle. It is shown that a possibility to reduce the noise emission by using pitch angle control. It is important to find the suitable pitch angle for optimal noise control, in order to respect noise regulation an especially at the night for the purpose reduce negative impact on power production.

## REFERENCES

- AbdelSalam, A. and V. Ramalingam (2014). Wake prediction of horizontal axis wind turbine using Full rotor modeling . *Journal of Wind Engineering and Industrial Aerodynamics*. 7–19.
- Arakawa, J. and F. Oliver (2005). Numerical Approach for Noise Reduction of Wind Turbine Blade Tip with Earth Simulator. *Journal of the Earth Simulator*. 11–33.
- Beaumier (1994). Effect of Higher Harmonic Control on Helicopter Rotor Blade-Vortex Interaction Noise, Prediction and Initial Validation , Proc, AGARD FDP *Symposium on Aerodynamics and Aeroacoustics of Rotorcraft, CP552, Berlin, Germany*.10-13.
- Brooks, T. F. and D. S. Pope (1989). Airfoil self-noise and prediction, *NASA Reference Publication* 1218.
- Brooks, T. F., F. Thomas and H. Robert (1983). Progress in Rotor Broadband Noise Research, *Vertica*. 287-307.
- Burton, T. and D. Sharpeand (2001). Wind energy handbook. 531-553.
- Cho, T. C. Kim and D. Lee (2010). Acoustic measurement for 12% scaled model of NREL Phase VI wind turbine, *Current Applied Physics Paper*. S320–S325.
- Fowes Williams, J. E. and D. L. Hawkings (1996). Sound generation by turbulence and surfaces in arbitrary motion, *Philos Trans-act AMath PhysEngSci*, 321-42.
- Göçmen, T. and B. Özerdem (2012). Airfoil optimization for noise emission problem and aerodynamic performance criterion on small scale wind turbines, *Energy*. 62–71.
- Gruber, M., P. Joseph and T. P. Chong (2010). Experimental Investigation of Airfoil Self Noise and Turbulent Wake Reduction by the use of Trailing Edge Serrations, *Proceedings of the 16th AIAA/CEAS Aeroacoustics Conference*.
- Gwang-Se, L. and C. H. Cheolung (2013). A case study of localization and identification of noise sources from a pitch and a stall regulated wind turbine, *Applied Acoustics*. 817-827.
- Herr, M. (2006). Experimental study on noise reduction through trailing edge brushes. New Results in Numerical and Experimental Fluid Mechanics V, Notes on Numerical Fluid Mechanics and Multidisciplinary Design. 92, 365-372.
- Jang-oh, M. and L. Young-ho (2011). Numerical simulation for prediction of aerodynamic noise characteristics on a HAWT of NREL phase VI, *Mechanical Science and Technology*. 1341-1349.
- Leloudas, G. and W. J. Zhu Sørensen (2007). Prediction and Reduction of Noise from a 2.3 MW Wind Turbine, *Journal of Physics, Conference Series* 75, 012083.
- Lighthill, M. J. (1952). On Sound generated aerodynamically General theory, *Proc RoySoc London SerA* .564-87.
- Menter, F. R. (1994). Two-equation eddy-viscosity model for engineering applications, *AIAA paper*. 1598-1605.
- Moreau, D. J. and L. A. Brooks and C. J. Doolan (2011). Flat plate self-noise reduction at low to moderate Reynolds number with trailing edge serrations, Proceedings on Acoustics, Gold Coast, Australia. Queensland, *Australian Acoustical Society*.
- Oerlemans, S. (2008). Reduction of wind turbine noise using optimized airfoils and trailing-edge serrations. 14th AIAA/CEAS Aeroacoustics Conference. Vancouver, Canada.
- Oerlemansa, S. and P. Sijtsma (2007). Location and quantification of noise sources on a wind turbine, *Journal of Sound and Vibration*. 869–883.
- Sahan, H. Wasala and C. Rupert (2015). Aeroacoustic noise prediction for wind turbines using Large Eddy Simulation, *Journal of Wind Engineering and Industrial Aerodynamics* .17–29.
- Schepers, J. G. (1997). Field rotor aerodynamics Final report of IEA Annex XIV, ECN-C-97-027, *Energy Research Center of the Netherlands*.
- Schultz, K. (1994). Aeroacoustic Calculation of Helicopter Ro-tors at DLR.Proc, *AGARD FDP Symposium on Aerodynamics and Aeroacoustics of Rotorcraft, CP552, Berlin, Germany*.10-13.
- Shaltout, M. L. and D. Chen (2013). Optimal control of a wind turbine for tradeoff analysis between energy harvesting and noise emission, Proceedings of the ASME, *Dynamic Systems and Control Conference*, Palo Alto (CA).
- Simms, D. A., S. Schreck and M. L. Fingersh (2001). NREL unsteady aerodynamics experiment in the NASA-Ames wind tunnel: a comparison of predictions to measurements. In: National Renewable Energy Laboratory Colorado, USA.
- Spalart, P.(2000). Strategies for turbulence modeling and simulations, *International Journal of Heat and Fluid Flow* 252–263.
- Tadamasa, A. and M. Zangeneh (2011). Numerical prediction of wind turbine noise, *Renewable Energy* 1902-1912.
- Wagne, S. and R. Bareiss (1996). Wind turbine noise, *Springer*.

